THE JOURNAL OF PHYSICAL CHEMISTRY Letters

Letter

Cite This: J. Phys. Chem. Lett. 2019, 10, 2739−2744

pubs.acs.org/JPCL

Defect Healing in Layered Materials: A Machine Learning-Assisted Characterization of MoS_2 Crystal Phases

Sungwook Hong,[†] Ken-ichi Nomura,[†] Aravind Krishnamoorthy,[†] Pankaj Rajak,[⊥] Chunyang Sheng,[†] Rajiv K. Kalia,[†] Aiichiro Nakano,[†] and Priya Vashishta*[,†]

[†]Collaboratory for Advanced Computing and Simulations, Department of Physics & Astronomy, Department of Computer Science, Department of Chemical Engineering & Materials Science, and Department of Biological Sciences, University of Southern California, Los Angeles, California 90089-0242, United States

[⊥]Argonne Leadership Computing Facility, Argonne National Laboratory, Argonne, Illinois 60439, United States

Supporting Information

ABSTRACT: Monolayer MoS_2 is an outstanding candidate for a next-generation semiconducting material because of its exceptional physical, chemical, and mechanical properties. To make this promising layered material applicable to nanostructured electronic applications, synthesis of a highly crystalline MoS_2 monolayer is vitally important. Among different types of synthesis methods, chemical vapor deposition (CVD) is the most practical way to synthesize few- or mono-layer MoS_2 on the target substrate owing to its simplicity and scalability. However, synthesis of a highly crystalline MoS_2 layer remains elusive. This is because of the number of grains and defects unavoidably generated during CVD synthesis. Here, we perform multimillion-atom reactive molecular dynamics (RMD) simulations to identify an origin of the grain growth, migration, and defect healing process on a CVD-grown MoS_2 monolayer. RMD results reveal that grain boundaries could be successfully repaired by multiple heat treatments. Our work proposes a new way of controlling the grain growth and migration on a CVD-grown MoS_2 monolayer.

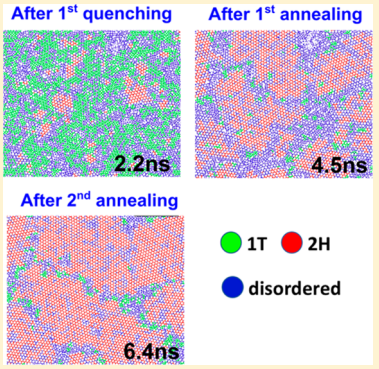

Graphene and other two-dimensional materials have allowed the exploration of novel layered and stacked nanostructures with remarkable functionality.[1−3] In particular, molybdenum disulfide (MoS_2), one of the archetypal transition-metal dichalcogenide (TMDC) materials, has received great attention owing to its unique physical, chemical, and mechanical properties.[4] For example, MoS_2 monolayer has a high band gap (∼1.8 eV), high carrier mobility, and exceptional mechanical strength in comparison to its bulk counterpart or other conventional Si-based materials.[5−9] These characteristics allow the MoS_2 monolayer to be applicable to the next-generation semiconducting-related applications such as ultrathin channel materials and/or flexible thin transistors.[10,11] In addition, MoS_2 layers with sulfur vacancies act as catalysts for the electrochemical hydrogen evolution reaction.[12] To bring this promising layered TMDC material into mass production, numerous efforts have been made, including physical vapor deposition, mechanical exfoliation, hydrothermal synthesis, and chemical vapor deposition (CVD).[10,13]

Among these techniques, CVD is the most practical and scalable way to synthesize large-scale and high-quality MoS_2 layers on the target substrate.[14,15] Consequently, many researchers have reported mechanistic studies on CVD synthesis of TMDC materials using experimental[16−19] and computational[20−22] approaches, and these studies have greatly improved our understanding of reaction mechanisms for the CVD reaction processes. That is, the replacement of O atoms in MoO_3 reactants with S atoms in the sulfur precursors is the key reaction step for synthesis of the MoS_2 layer during CVD synthesis. Unfortunately, the number of grains and line defects are intrinsically formed during CVD synthesis,[23−25] which could degrade the electrical or mechanical performance.[26−28] To repair these grain boundaries and defects, a few post-treatments have been experimentally suggested, such as a postdeposition sulfurization annealing,[29] thermal annealing,[30] laser heating,[31] and electron beam irradiation.[32] As such, it is essential to investigate effective post-sulfurization strategies for CVD synthesis toward higher-quality TMDC materials.

However, optimal conditions for CVD synthesis of highly crystalline MoS_2 layers have yet to be fully investigated. This is primarily because the degree to which a high crystallinity of MoS_2 layer is achieved has not been fully understood, and the obtained information primarily relies on a trial-and-error experimental approach. Here, we perform multimillion-atom reactive molecular dynamics (RMD) simulations, which allow us to gain an atomic scale insight into reaction dynamics of complex nanostructured materials[33] to investigate the origin of the formation of grains and line defects and their healing process on CVD-grown MoS_2 monolayer. Our RMD simulations are based on the first-principles-informed

Received: February 13, 2019
Accepted: May 3, 2019
Published: May 3, 2019

DOI: 10.1021/acs.jpclett.9b00425
J. Phys. Chem. Lett. 2019, 10, 2739−2744

ReaxFF[34] reactive force field, which was previously used and validated for CVD synthesis reactions.[22,35] In addition, RMD trajectories were characterized by our newly developed machine learning algorithm to identify local atomic structures. Below, we report results of our RMD simulations, followed by conclusions of this work and details of our simulation setup.

To efficiently conduct presulfurization of the MoO_3 slab followed by post quenching−annealing simulations, we first prepared a presulfurized MoO_xS_y slab using a relatively small system (Figure 1a). The detailed system configuration and

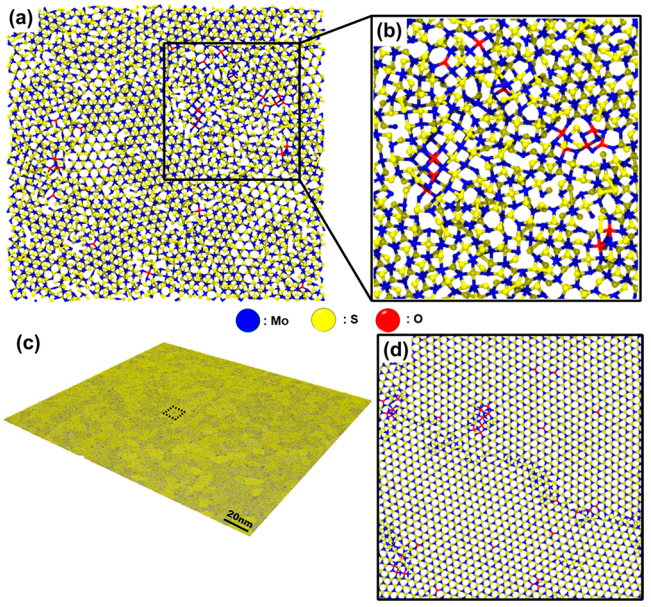

Figure 1. Snapshot of MoS_2 monolayer used in this work: (a) Presulfurized MoO_xS_y surface with a relatively small size of 10.5 nm by 9.8 nm in the *x*- and *y*-directions, respectively. (b) An enlarged image of the MoO_xS_y surface in panel a showing that the surface was most likely sulfurized while its crystallinity is poor at this moment. (c) Final snapshot of the expanded MoO_xS_y surface structure using the surface structure in panel a (211.0 nm × 196.3 nm in the *x*- and *y*-directions, respectively) after multimillion-atom RMD simulations of the postquenching−annealing steps. (d) Enlarged image of the MoO_xS_y surface highlighted by the black-dotted square in panel c. Note that the surface crystallinity is greatly improved, compared with the structure in panel a, by the quenching−annealing steps.

simulations schedule for the presulfurization step of the MoO_3 slab are discussed in the Supporting Information, and Movie S1 shows the reaction dynamics of the sulfurization of the MoO_3 slab using S_2 precursors. It should be noted that the different S/Mo ratios in the system affect only the reduction/sulfidation rate of MoO_3 structure while the key reaction steps for reduction and sulfidation processes remain the same. This was confirmed by our previous studies.[22,35] After this presulfurization step, the initial MoO_3 slab was most likely reduced and sulfurized. That is, the presulfurized MoO_xS_y surface contains a relatively small portion of O atoms, when compared with that of S atoms (Figure 1b). Note that reaction mechanisms for the reduction and sulfurization processes were also discussed in our previous work.[22,35] The presulfurized MoO_xS_y surface was obtained at high temperatures (3000 K) so that the surface structure is quite disordered at this time. We then expanded this structure (replicated in 20 times by 20 times in the *x*- and *y*-directions, respectively) and performed multimillion-atom RMD simulations (4,305,600 atoms in total) of quenching−annealing steps in the following schedule: (1) quenching from 3000 K to 1000K for 1.0 ns; (2) two annealing cycles consisting of a heating step from 1000 K to 1600 K for 0.4 ns followed by a thermalization step at 1600 K for 1.5 ns and a cooling step from 1600 K to 1000 K for 0.4 ns.

Prior to these quenching−annealing steps, the expanded surface structure was also thermalized at 3000 K for 1.0 ns to randomly distribute local atomic structures on the entire surface. The final configuration of the expanded MoO_xS_y surface and its enlarged image are shown in panels c and d of Figure 1, respectively. Interestingly, the postquenching−annealing steps improve the crystallinity of the MoO_xS_y surface (see Panels a and d of Figure 1 for comparison). Panels a, b, and c of Figure 2 show time evolutions of local atomic

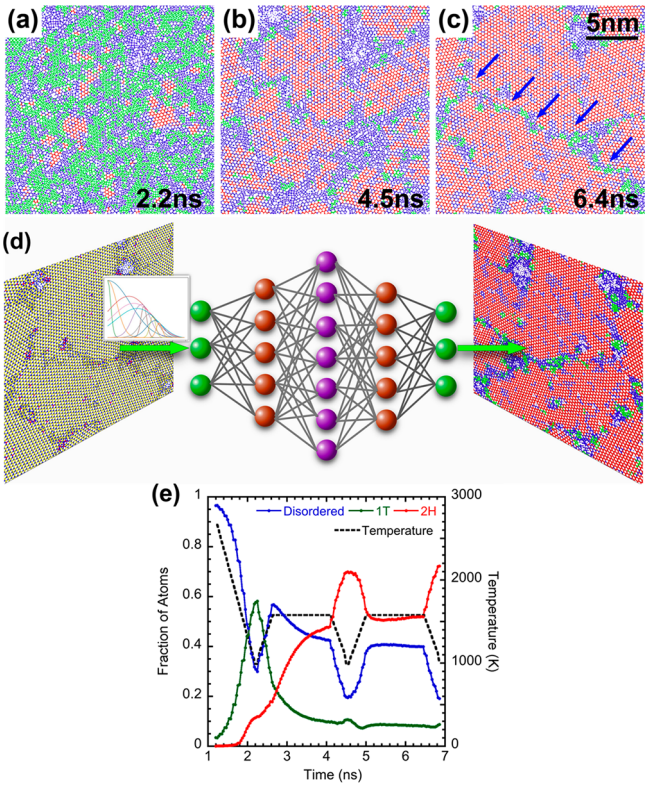

Figure 2. Local atomic structures (a) after the initial quenching at 2.2 ns, (b) after the first annealing at 4.5 ns, and (c) after the second annealing at 6.4 ns. Note that blue, green, and red colors represent disordered-, 1T-, 2H- phases of MoS_2, respectively. In addition, the blue arrows in panel c indicate the grain boundaries or line defects consisting of disordered- and 1T-phases, evolved during the quenching−annealing steps. (d) Schematic of a three-layer neural network model for defect identification in layered TMDC materials. (e) Temperature cycle profile during the entire RMD schedule (the black dotted curve) and time evolution of the local atomic structures based on the machine learning-assisted characterization.

structures on a small portion of the entire surface in Figure 1c at 2.2, 4.5, and 6.4 ns, respectively. Basically, TMDC exists in two distinct crystal structures, which are 2H and 1T. These TMDCs also contain grain boundaries or line defects in their crystalline phases.[26]

As shown in Figure 2, the local atomic structures were identified by three phases: disordered (blue), 1T (green), and 2H (red) using machine learning characterization;[36] in this work, we built a feed-forward neural network model with three

DOI: 10.1021/acs.jpclett.9b00425
J. Phys. Chem. Lett. 2019, 10, 2739−2744

hidden layers (Figure 2d) to identify the different phases present in MoS_2 crystal. The machine learning algorithm is further discussed in the Supporting Information. We then quantified the three phases for the entire simulation schedule along with the temperature profile. Figure 2e suggests that the initial surface consists of almost disordered phases, indicating the presulfurized MoO_xS_y surface at high temperatures was highly amorphous. However, after the initial quenching step (up to 2.2 ns), a majority of disordered structures converted to the 1T crystal-phase; consequently, this 1T-phase further transformed into 2H crystal-phase during the first (2.2−4.5 ns) and second (4.5−6.4 ns) annealing steps. Namely, the 1T- and disordered-phases transformed into the 2H-crystal phase by applying successive heat-up/thermalization steps, thus expanding the area of the 2H-crytal phase. These results suggest that the quenching and annealing steps are very effective ways to activate structural transformation on the MoS_2 layers after CVD synthesis, which was also suggested by the thermal annealing and postlaser heating experiments.[30,31] In addition, during the quenching−annealing steps, grain boundaries were developed along with the disordered- and 1T-phases while the remaining portion of the surface primarily consists of 2H-phase (see the blue arrows in Figure 2c). The observation and evolution of the grain boundaries are discussed in the following section.

Grain Growth, Migration, and Defect Healing. To further clarify the grain growth, migration, and intergrain interactions during the quenching−annealing steps, we expanded our machine learning-based analysis of the local atomic configuration to the entire slab. After the first quenching step, a large number of Mo and S atoms construct the disordered and 1T phases. We also observed the nucleation of a highly crystalline 2H-phase (see red regions randomly distributed in Figure 3a).

After the first annealing, the 2H-phase grains grow further, and grain boundaries are developed, made of the disordered- and 1T-phase atomic structures discussed in the previous section (Figure 3b). During the second annealing (Figure 3c), the 2H-phase grains merge into bigger grains induced by heat treatments. Movie S2 shows the full dynamics of structural transformation between disordered and 1T/2H phases. Such a growth and migration of grains could be further understood and confirmed by Figure 3d−f, which are characterized by grain IDs at 2.2, 4.1, and 6.4 ns, respectively. On the basis of these characterizations, we found that the crystallinity of the MoS_2 surface was improved by active grain growth and grain boundary migration and combination. Panels g and h of Figure 3 clarify the number of grains and maximum grain size, respectively. The number of grains decreases while the maximum size of grains increases during the quenching−annealing steps. Given the results above, proper heat treatments allow small grains to interact with each other, merging into a bigger grain, thus leading to a decrease in line defects.

Mechanisms of Structural Transformation. This transient formation of the 1T-phase MoS_2 structure along the crystallization pathway is unexpected because of the metastability of the 1T-phase relative to the 2H-phase structure. To understand this unusual mechanism, we have performed density functional theory (DFT)-based nudged elastic band (NEB) calculations of energy barriers involved in the homogeneous phase transformation between 2H and 1T crystal structures of MoS_2. NEB simulations were performed for MoS_2 crystals at two densities, ρ = 0.306 μg cm^{-2},

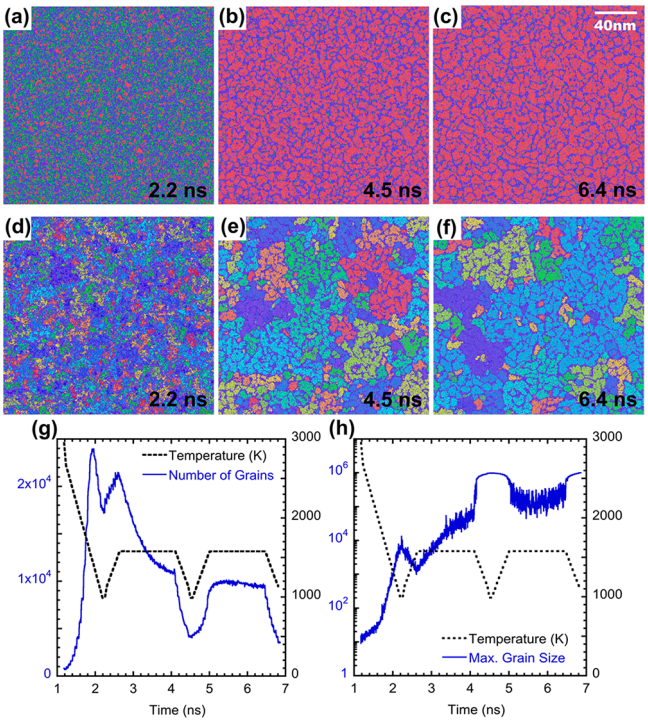

Figure 3. Structural transformation of MoO_xS_y surface during annealing cycles: (a−c) snapshots of the surface structures characterized by structure IDs (i.e., disordered, 1T, and 2H phases) after the initial quenching (2.2 ns), the first annealing (4.5 ns), and the second annealing (6.4 ns), respectively; (d−f) snapshots of the surface structures characterized by grain IDs after the initial quenching (2.2 ns), the first annealing (4.5 ns), and the second annealing (6.4 ns), respectively; (g and h) time evolution of the number of grains and the maximum grain size, respectively. Note that surface structure was crystallized by grain growth and migration, resulting in a bigger grain size during quenching−annealing steps while decreasing the number of grains. For further information on the characterization of the structure and grain IDs, see the Supporting Information.

corresponding to the normal crystal density in the ground state, and ρ = 0.404 μg cm^{-2}, corresponding to the higher density encountered in our synthesis pathway (Figure 4a). The homogeneous phase transformation pathway involves the translation of one plane of S atoms by half a lattice constant along the armchair direction (Figure 4b) and provides an upper bound for the energy barrier of the structural phase transformation, which mainly takes place via migration of zigzag phase boundaries.[37,38] Figure 4a shows that at the nominal crystal density, the 2H crystal structure is more stable than the 1T polytype by 0.83 eV/formula unit. In contrast, at the higher density of ρ = 0.404 μg cm^{-2}, encountered in CVD growth processes in our RMD simulations (see Figure S1 in the Supporting Information), the 2H crystal is metastable relative to the 1T phase by 0.08 eV and the homogeneous phase transformation barrier is reduced significantly to only 0.21 eV/formula unit (~900k_B per atom). Therefore, early stage sulfidation processes at high density are characterized by the transient formation of the 1T MoS_2 crystal structure.

In conclusion, we investigated the origin of the grain growth, migration, and defect healing during the quenching−annealing steps using multimillion-atom RMD simulations. Our RMD trajectories were uniquely characterized by the newly developed machine learning algorithm to quantify the local

DOI: 10.1021/acs.jpclett.9b00425
J. Phys. Chem. Lett. 2019, 10, 2739−2744

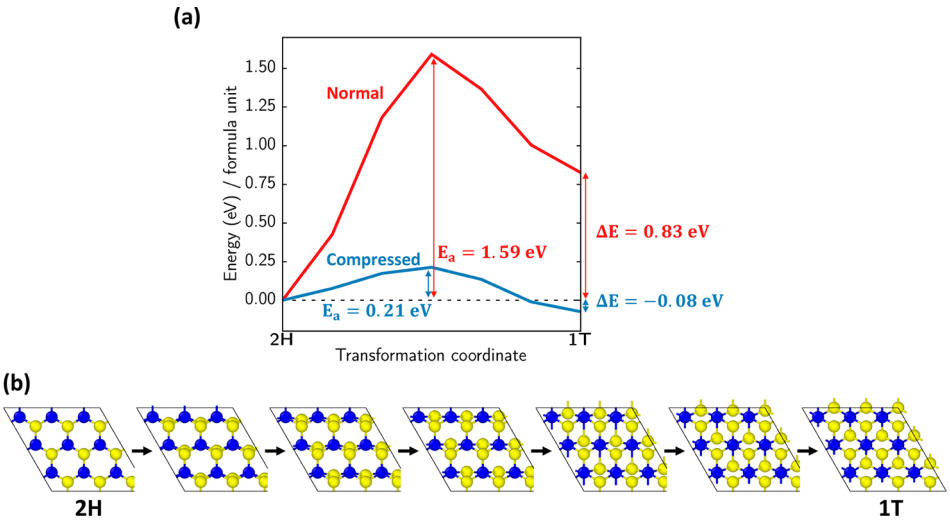

Figure 4. Energy barriers for the homogeneous phase transformation between the 2H and 1T crystal structures of MoS_2 at two representative densities, ρ = 0.306 μg cm^{-2} and ρ = 0.404 μg cm^{-2}. (a) At nominal crystal densities, the large phase transformation barriers (~1.59 eV) prevent the formation of the 1T-phase, whereas the formation of the 1T-phase is facile at the higher densities, encountered in the RMD simulations, because of the significantly reduced barriers (~0.21 eV). (b) The 2H → 1T representative homogeneous phase transformation pathway involves the translation of one plane of the S atoms along the armchair direction. This translation transforms the trigonal prismatic coordination around the central Mo atoms to octahedral coordination (blue, Mo atoms; yellow, S atoms).

atomic structures on the presulfurized MoO_xS_y surface. Our RMD results assisted by the machine learning analysis reveal that the 2H-phase grains were randomly nucleated on the surface and that grain boundaries, consisting of disordered or 1T-phases structures, are grown. After that, the 2H-phase grains interact with each other, merging into bigger grains, thereby healing the line defects. All of these behaviors were induced and activated by the quenching−annealing steps. These atomic scale mechanisms for the structure transformation were further supported by our DFT calculations. These RMD results suggest that multiple heating−cooling cycles on the post-CVD growth may play an important role in the synthesis of high-quality MoS_2 layers. As such, our work provides a new method of grain and crystallinity control in layered materials, helping to guide the synthesis of higher-quality layered 2D materials for nanostructured applications.

Our computational model for RMD simulations consists of 4,305,600 atoms in total: 1,497,600 O atoms, 2,347,200 S atoms, and 460,800 Mo atoms. The system dimensions are 211.0 × 196.3 × 14.5 (nm^3) in the *x*-, *y*-, and *z*-directions, respectively, and one RMD time step is 0.75 fs. To describe Mo−O−S interactions, highly accurate ReaxFF reactive force field parameters were taken from Hong et al.[22] Our ReaxFF force field parameters qualitatively reproduce critical reaction steps for CVD synthesis of the MoS_2 layer (i.e., O_2 evolution and SO/SO_2 formation), which were validated through experimental literature and DFT calculations. Our ReaxFF force field parameters were previously trained against a comprehensive quantum mechanics training set. In particular, our ReaxFF force field parameters mimic the overall trend in stability of MoS_2 structures as well as structural behaviors of MoS_2 and MoO_3 crystals.[35] In addition, our ReaxFF force field has the ability to reasonably describe CVD growth and the formation of 1T phase and its transition to 2H phase during RMD simulations. To model the support from the substrate, we apply a one-dimensional harmonic potential from the middle of the MD system in the *z*-direction on Mo atoms. The spring constant is 75 kcal/Å^2, which sufficiently contains Mo atoms within a thin slab with elevated temperature. To facilitate the sulfurization reaction process, S and O atoms are also subjected to a spring force with the spring constant of 1 kcal/Å^2. This guiding force is applied to move S atoms toward the Mo and O atoms away from the slab. The guiding forces are applied on S atoms every 200 RMD steps and O atoms for 100 RMD steps, i.e., 150 and 75 fs, respectively. To control the system temperature, velocities of all atoms were rescaled every 100 steps to the target temperature. This scaling scheme reproduces the key reaction steps during CVD synthesis, consistent with our previous work that used the *NVT* ensemble with a Nose−Hoover thermostat.[22,35] Our multimillion-atom RMD simulations were performed using 524,288 IBM BlueGene/Q cores on Mira and Intel Xeon Knights Landing (KNL) 262,144 cores on Theta at Argonne Leadership Computing Facility. Phase-transformation activation energy barriers, equal to the difference between the energy of the 2H-phase crystal structure and the saddle-point configuration along the 2H−1T phase transition pathway, were calculated using the climbing image nudged elastic band (CI-NEB) method implemented in the Vienna ab Initio Simulation Package (VASP) Transition State Tools code.[39] CI-NEB simulations were performed on 3 × 3 monolayer simulation cells containing 27 atoms. Simulation cells are separated from their periodic images in the out-of-plane direction by a 15 Å vacuum. DFT energies for each image in the phase transformation pathway are calculated using DFT with the Perdew−Burke−Ernzerhof form of the generalized gradient approximation to the exchange−correlation functional.[40] Valence electron wave functions are constructed using a plane wave basis set containing components up to a kinetic energy of 400 eV, and the reciprocal space is sampled using a 3 × 3 × 1 Γ-centered mesh with a Gaussian smearing of orbital occupancies of 0.1 eV. DFT simulations were performed with the projector augmented wave[41] method implemented in VASP.[42,43]

DOI: 10.1021/acs.jpclett.9b00425
J. Phys. Chem. Lett. 2019, 10, 2739−2744

■ ASSOCIATED CONTENT

Supporting Information

The Supporting Information is available free of charge on the ACS Publications website at DOI: 10.1021/acs.jpclett.9b00425.

Details about the molecular dynamics schedule for presulfurization of the MoO_3 slab (section S1), characterization and analysis of local crystal structure and grain ID (section S2), changes in mass density of the partially sulfidized MoO_xS_y surface (section S3), and description of the neural network model for defect characterization (section S4) (PDF)

Reaction dynamics of sulfurization of MoO_3 slab using S_2 precursors (Movie S1) (MOV)

Full dynamics of structural transformation between disordered and 1T/2H phases (Movie S2) (MOV)

■ AUTHOR INFORMATION

Corresponding Author

*E-mail: priyav@usc.edu.

ORCID

Sungwook Hong: 0000-0003-3569-7701
Aravind Krishnamoorthy: 0000-0001-6778-2471
Pankaj Rajak: 0000-0002-6344-6056
Aiichiro Nakano: 0000-0003-3228-3896
Priya Vashishta: 0000-0003-4683-429X

Notes

The authors declare no competing financial interest.

■ ACKNOWLEDGMENTS

This work was supported as part of the Computational Materials Sciences Program funded by the U.S. Department of Energy, Office of Science, Basic Energy Sciences, under Award Number DE-SC0014607. The simulations were performed at the Argonne Leadership Computing Facility under the DOE INCITE and Aurora Early Science programs and at the Center for High Performance Computing of the University of Southern California.

■ REFERENCES

(1) Geim, A. K.; Grigorieva, I. V. Van der Waals Heterostructures. *Nature* **2013**, *499*, 419−425.

(2) Ashton, M.; Paul, J.; Sinnott, S. B.; Hennig, R. G. Topology-Scaling Identification of Layered Solids and Stable Exfoliated 2D Materials. *Phys. Rev. Lett.* **2017**, *118*, 106101.

(3) Son, Y.-W.; Cohen, M. L.; Louie, S. G. Energy Gaps in Graphene Nanoribbons. *Phys. Rev. Lett.* **2006**, *97*, 216803.

(4) Lee, Y. H.; Zhang, X. Q.; Zhang, W.; Chang, M. T.; Lin, C. T.; Chang, K. D.; Yu, Y. C.; Wang, J. T. W.; Chang, C. S.; Li, L. J.; et al. Synthesis of Large-Area MoS_2 Atomic Layers with Chemical Vapor Deposition. *Adv. Mater.* **2012**, *24*, 2320−2325.

(5) Lembke, D.; Kis, A. Breakdown of High-Performance Monolayer MoS_2 Transistors. *ACS Nano* **2012**, *6*, 10070−10075.

(6) Mak, K. F.; Lee, C.; Hone, J.; Shan, J.; Heinz, T. F. Atomically Thin MoS_2: A New Direct-Gap Semiconductor. *Phys. Rev. Lett.* **2010**, *105*, 136805.

(7) Ganatra, R.; Zhang, Q. Few-layer MoS_2: A Promising Layered Semiconductor. *ACS Nano* **2014**, *8*, 4074−4099.

(8) Kaplan, D.; Gong, Y.; Mills, K.; Swaminathan, V.; Ajayan, P.; Shirodkar, S.; Kaxiras, E. Excitation Intensity Dependence of Photoluminescence from Monolayers of MoS_2 and WS_2/MoS_2 Heterostructures. *2D Mater.* **2016**, *3*, 015005.

(9) Mortazavi, B.; Ostadhossein, A.; Rabczuk, T.; Van Duin, A. C. T. Mechanical Response of All-MoS_2 Single-Layer Heterostructures: A ReaxFF Investigation. *Phys. Chem. Chem. Phys.* **2016**, *18*, 23695−23701.

(10) Venkata Subbaiah, Y.; Saji, K.; Tiwari, A. Atomically Thin MoS_2: A Versatile Nongraphene 2D Material. *Adv. Funct. Mater.* **2016**, *26*, 2046−2069.

(11) Gupta, A.; Sakthivel, T.; Seal, S. Recent Development in 2D materials Beyond Graphene. *Prog. Mater. Sci.* **2015**, *73*, 44−126.

(12) Li, H.; Du, M.; Mleczko, M. J.; Koh, A. L.; Nishi, Y.; Pop, E.; Bard, A. J.; Zheng, X. Kinetic Study of Hydrogen Evolution Reaction Over Strained MoS_2 with Sulfur Vacancies Using Scanning Electrochemical Microscopy. *J. Am. Chem. Soc.* **2016**, *138*, 5123−5129.

(13) Lv, Z.; Mahmood, N.; Tahir, M.; Pan, L.; Zhang, X.; Zou, J.-J. Fabrication of Zero to Three Dimensional Nanostructured Molybdenum Sulfides and Their Electrochemical and Photocatalytic Applications. *Nanoscale* **2016**, *8*, 18250−18269.

(14) Yu, J.; Li, J.; Zhang, W.; Chang, H. Synthesis of High Quality Two-Dimensional Materials via Chemical Vapor Deposition. *Chem. Sci.* **2015**, *6*, 6705−6716.

(15) Zhan, Y.; Liu, Z.; Najmaei, S.; Ajayan, P. M.; Lou, J. Large-Area Vapor-Phase Growth and Characterization of MoS_2 Atomic Layers on a SiO_2 Substrate. *Small* **2012**, *8*, 966−971.

(16) Jeon, J.; Lee, J.; Yoo, G.; Park, J.-H.; Yeom, G. Y.; Jang, Y. H.; Lee, S. Size-Tunable Synthesis of Monolayer MoS_2 Nanoparticles and Their Applications in Non-Volatile Memory Devices. *Nanoscale* **2016**, *8*, 16995−17003.

(17) Schmidt, H.; Wang, S.; Chu, L.; Toh, M.; Kumar, R.; Zhao, W.; Castro Neto, A.; Martin, J.; Adam, S.; Özyilmaz, B.; et al. Transport Properties of Monolayer MoS_2 Grown by Chemical Vapor Deposition. *Nano Lett.* **2014**, *14*, 1909−1913.

(18) Zhu, D.; Shu, H.; Jiang, F.; Lv, D.; Asokan, V.; Omar, O.; Yuan, J.; Zhang, Z.; Jin, C. Capture the Growth Kinetics of CVD Growth of Two-Dimensional MoS_2. *npj 2D Mater. Appl.* **2017**, *1*, 8.

(19) Salazar, N.; Beinik, I.; Lauritsen, J. V. Single-layer MoS_2 Formation by Sulfidation of Molybdenum Oxides in Different Oxidation States on Au (111). *Phys. Chem. Chem. Phys.* **2017**, *19*, 14020−14029.

(20) Shi, X.-R.; Wang, J.; Hermann, K. Theoretical Cluster Studies on the Catalytic Sulfidation of MoO_3. *J. Phys. Chem. C* **2010**, *114*, 6791−6801.

(21) Misawa, M.; Tiwari, S.; Hong, S.; Krishnamoorthy, A.; Shimojo, F.; Kalia, R. K.; Nakano, A.; Vashishta, P. Reactivity of Sulfur Molecules on MoO_3 (010) Surface. *J. Phys. Chem. Lett.* **2017**, *8*, 6206−6210.

(22) Hong, S.; Sheng, C.; Krishnamoorthy, A.; Rajak, P.; Tiwari, S. C.; Nomura, K.; Misawa, M.; Shimojo, F.; Kalia, R. K.; Nakano, A.; et al. Chemical Vapor Deposition Synthesis of MoS_2 Layers from the Direct Sulfidation of MoO_3 Surfaces Using Reactive Molecular Dynamics Simulations. *J. Phys. Chem. C* **2018**, *122*, 7494−7503.

(23) Wang, Q. H.; Kalantar-Zadeh, K.; Kis, A.; Coleman, J. N.; Strano, M. S. Electronics and optoelectronics of two-dimensional transition metal dichalcogenides. *Nat. Nanotechnol.* **2012**, *7*, 699−712.

(24) Lin, Z.; Carvalho, B. R.; Kahn, E.; Lv, R.; Rao, R.; Terrones, H.; Pimenta, M. A.; Terrones, M. Defect Engineering of Two-Dimensional Transition Metal Dichalcogenides. *2D Mater.* **2016**, *3*, 022002.

(25) Yazyev, O. V.; Chen, Y. P. Polycrystalline Graphene and Other Two-Dimensional Materials. *Nat. Nanotechnol.* **2014**, *9*, 755−767.

(26) Wang, S.; Lee, G.-D.; Lee, S.; Yoon, E.; Warner, J. H. Detailed Atomic Reconstruction of Extended Line Defects in Monolayer MoS_2. *ACS Nano* **2016**, *10*, 5419−5430.

(27) Sengupta, A.; Saha, D.; Niehaus, T. A.; Mahapatra, S. Effect of Line Defects on the Electrical Transport Properties of Monolayer MoS_2 Sheet. *IEEE Trans. Nanotechnol.* **2015**, *14*, 51−56.

(28) Wu, J.; Cao, P.; Zhang, Z.; Ning, F.; Zheng, S.; He, J.; Zhang, Z. Grain-Size-Controlled Mechanical Properties of Polycrystalline Monolayer MoS_2. *Nano Lett.* **2018**, *18*, 1543−1552.

(29) Ishihara, S.; Hibino, Y.; Sawamoto, N.; Suda, K.; Ohashi, T.; Matsuura, K.; Machida, H.; Ishikawa, M.; Sudoh, H.; Wakabayashi,

DOI: 10.1021/acs.jpclett.9b00425
J. Phys. Chem. Lett. 2019, 10, 2739−2744

H.; et al. Improving Crystalline Quality of Sputtering-Deposited MoS_2 Thin Film by Postdeposition Sulfurization Annealing Using $(t\text{-}C4H9)_2S_2$. *Jpn. J. Appl. Phys.* **2016**, *55*, 04EJ07.
(30) Eda, G.; Yamaguchi, H.; Voiry, D.; Fujita, T.; Chen, M.; Chhowalla, M. Photoluminescence from Chemically Exfoliated MoS_2. *Nano Lett.* **2011**, *11*, 5111−5116.
(31) McConney, M. E.; Glavin, N. R.; Juhl, A. T.; Check, M. H.; Durstock, M. F.; Voevodin, A. A.; Shelton, T. E.; Bultman, J. E.; Hu, J.; Jespersen, M. L.; et al. Direct Synthesis of Ultra-Thin Large Area Transition Metal Dichalcogenides and Their Heterostructures on Stretchable Polymer Surfaces. *J. Mater. Res.* **2016**, *31*, 967−974.
(32) Kim, B. H.; Gu, H. H.; Yoon, Y. J.; et al. Atomic Rearrangement of a Sputtered MoS_2 Film from Amorphous to a 2D Layered Structure by Electron Beam Irradiation. *Sci. Rep.* **2017**, *7*, 3874.
(33) Mo, Y.; Turner, K. T.; Szlufarska, I. Friction Laws at the Nanoscale. *Nature* **2009**, *457*, 1116−1119.
(34) van Duin, A. C. T.; Dasgupta, S.; Lorant, F.; Goddard, W. A. ReaxFF: A Reactive Force Field for Hydrocarbons. *J. Phys. Chem. A* **2001**, *105*, 9396−9409.
(35) Hong, S.; Krishnamoorthy, A.; Rajak, P.; Tiwari, S. C.; Misawa, M.; Shimojo, F.; Kalia, R. K.; Nakano, A.; Vashishta, P. Computational Synthesis of MoS_2 Layers by Reactive Molecular Dynamics Simulations: Initial Sulfidation of MoO_3 Surfaces. *Nano Lett.* **2017**, *17*, 4866−4872.
(36) Goodfellow, I.; Bengio, Y.; Courville, A.; Bengio, Y. *Deep learning*; MIT Press: Cambridge, MA, 2016.
(37) Zhao, W.; Ding, F. Energetics and Kinetics of Phase Transition Between a 2H and a 1T MoS_2 Monolayer—A Theoretical Study. *Nanoscale* **2017**, *9*, 2301−2309.
(38) Lin, Y.-C.; Dumcenco, D. O.; Huang, Y.-S.; Suenaga, K. Atomic Mechanism of the Semiconducting-to-Metallic Phase Transition in Single-Layered MoS_2. *Nat. Nanotechnol.* **2014**, *9*, 391−396.
(39) Henkelman, G.; Uberuaga, B. P.; Jónsson, H. A climbing Image Nudged Elastic Band Method for Finding Saddle Points and Minimum Energy Paths. *J. Chem. Phys.* **2000**, *113*, 9901−9904.
(40) Perdew, J. P.; Burke, K.; Ernzerhof, M. Generalized Gradient Approximation Made Simple. *Phys. Rev. Lett.* **1996**, *77*, 3865−3868.
(41) Blöchl, P. E. Projector Augmented-Wave method. *Phys. Rev. B: Condens. Matter Mater. Phys.* **1994**, *50*, 17953.
(42) Kresse, G.; Furthmüller, J. Efficient Iterative Schemes for Ab Initio Total-Energy Calculations Using a Plane-Wave Basis Set. *Phys. Rev. B: Condens. Matter Mater. Phys.* **1996**, *54*, 11169.
(43) Kresse, G.; Furthmüller, J. Efficiency of Ab-Initio Total Energy Calculations for Metals and Semiconductors Using a Plane-Wave Basis Set. *Comput. Mater. Sci.* **1996**, *6*, 15−50.

DOI: 10.1021/acs.jpclett.9b00425
J. Phys. Chem. Lett. 2019, 10, 2739−2744